BULLETIN OF THE POLISH ACADEMY OF SCIENCES
TECHNICAL SCIENCES, Vol. 66, No. 5, 2018
DOI: 10.24425/125334

# Synchronization of state-feedback-controlled doubly fed induction generator with the grid

M. SZYPULSKI and G. IWAŃSKI*

Institute of Control and Industrial Electronics, Warsaw University of Technology, 75 Koszykowa St., 00-662 Warszawa, Poland

**Abstract.** This paper presents state feedback control with a linear-quadratic regulator of a doubly fed induction generator. Resonant terms are added to the plant model in order to provide disturbance rejection and reference tracking. A new approach to controlling a parameter varying linear model of the induction machine is presented, allowing to apply a linear-quadratic regulator to the doubly fed induction generator. The control scheme described herein is suitable for the doubly fed induction generator operating under unbalanced stator voltage conditions, because the controller with resonant terms is built in the stationary αβ coordinate system. In it, the positive and negative symmetrical sequences have equal frequencies. The paper highlights specific problems associated with state feedback control of the doubly fed induction generator, i.e. the process of generator connection to an unbalanced grid. In contrast with classical voltage-oriented cascade control methods, in state feedback control of a stand-alone doubly fed induction generator there is no separate rotor current controller. This may cause over-current problem during DFIG synchronization with the grid which has been solved in this paper. Voltage synchronization and grid operation of the generator were tested in a laboratory rig with a 7.5 kW wound-rotor induction machine.

**Key words:** induction generators, linear-quadratic control, state feedback, synchronization.

## 1. Introduction

The doubly fed induction generator (DFIG) is utilized in modern renewable energy systems such as wind turbines and hydropower plants [1]. DFIG rotor windings are connected to a power converter by means of slip rings, and its stator is directly connected to the power grid. Provided that rotor speed is close to synchronous speed, the generator can be controlled by a power converter with considerably reduced power. This is the main reason for DFIG popularity in medium-size variable-speed power generation systems. Although DFIG is mostly used in wind energy conversion systems, it can also prove useful in hydro plants [2], combustion-engine-driven generators [3, 4] and flywheel energy storage systems [5].

Figure 1 shows a typical topology of a grid-connected DFIG, in which part of the control structure described in this paper is highlighted. Issues connected with the grid-side converter (GSC) are neglected in the paper because GSC does not influence the performance of the machine. It acts as an active filter/rectifier, for which control methods are well known in the literature.

Turbine control and superior power management should be treated only as an example because there are many possible DFIG system configurations, which are beyond the scope of the paper. This paper focuses on DFIG control without taking account of prime mover dynamics. Torque and power references

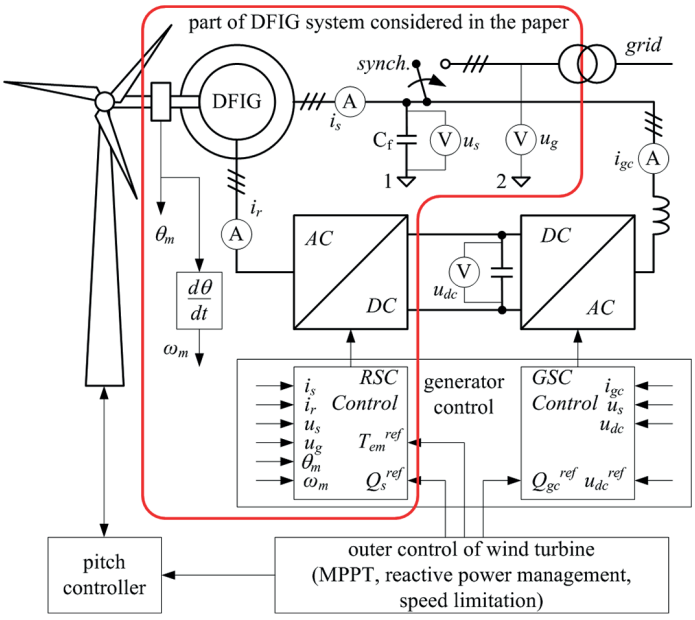


Fig. 1. Part of the wind-turbine-driven DFIG considered in the paper

for the generator controller come from superior power controllers, e.g. the maximum power point tracking (MPPT) algorithm [6]. This methodology has been used, for instance, in [1, 4] due to a significant difference in time constants between the primary source and generator.

The grid-connected DFIG is usually controlled with decoupled control loops in the synchronously rotating, field-oriented

*e-mail: iwanskig@isep.pw.edu.pl

Manuscript submitted 2017-07-27, revised 2018-01-08, initially accepted for publication 2018-02-12, published in October 2018.

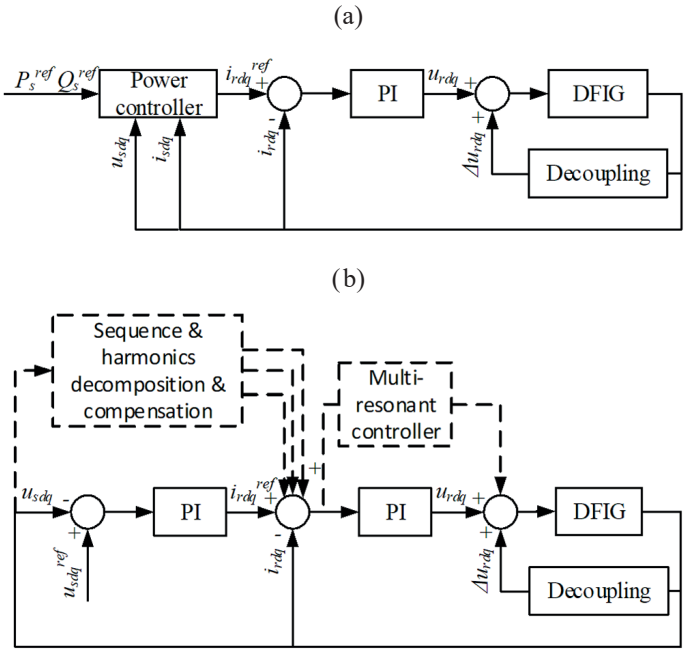


Fig. 2. DFIG control structures: a) decoupled cascade power control, b) decoupled cascade voltage control

(or voltage-oriented) coordinate system (Fig. 2a). Although these vector control methods provide satisfactory results with sinusoidal balanced grid voltage, they require modifications during voltage distortions and under unbalanced grid voltage conditions. Those can be obtained by means of calculating compensation terms and four controllers of rotor current symmetrical sequence components [7]. Another way is to use proportional-integral-resonant controllers in a rotating frame or proportional-resonant controllers in a stationary frame [8, 9] instead of separate controllers of the positive and negative sequence.

In [8], the authors assume fixed angular speed of the stator flux vector as well as constant phase shift between stator voltage and stator flux. Moreover, equation (24) derived in the paper remains true only for a balanced grid. In [9], the authors assume that the derivative of the stator voltage $\alpha$ component has the waveform of the $\beta$ component scaled by synchronous speed and, quite oppositely, the derivative of $\beta$ components has the waveform of the $\alpha$ component scaled by synchronous speed. This is true for specific unbalanced voltage conditions but in general $\alpha$ and $\beta$ components may have different amplitudes or phase shift different than 90 degrees as well. Thus, reference current calculated using this assumption does not produce the expected stator power for voltage unbalance.

Direct power control (DPC) is another control structure used in DFIG applications, described in [10–12]. However, when using vector control, the current harmonics are lower than when hysteresis controllers are used at the same average switching frequency [11]. This is because the resolution of the PWM signal created by the modulator in vector control is wider than the one created by the hysteresis controller in classic DPC. Additionally, in order to obtain any of the current reasonable targets (symmetrical stator current, sinusoidal rotor current or electromagnetic torque oscillations cancellation) in DPC methods, it is necessary to calculate adequate amplitude and phase of the power component oscillations. Although it is possible to introduce some factors allowing management of power component oscillations to obtain specific targets [12], lack of the current control inner loop hinders the implementation of current limitations in a simple manner. Compensation of electromagnetic torque oscillations during unbalanced grid operation can be arrived at as shown in [12]. However, although the decomposition of currents into positive and negative sequences can be neglected, grid voltage decomposition is usually necessary, as shown in [13].

Stand-alone DFIG usually contains additional superior stator voltage regulation loops, which create, together with current controllers, a cascade control scheme (Fig. 2b). Moreover, extra parallel regulators can be incorporated into the control system under non-linear load conditions. Tuning of DFIG controllers designed for unbalanced and distorted conditions can be especially problematic due to interferences of simultaneously operating parallel controllers. State feedback control is an approach to control system design different from the cascade scheme because overall plant dynamics are considered during individual tuning procedure calls. The paper presents full-state feedback control of DFIG with the rotor-side converter (RSC) for stand-alone and grid operation. A control method for stand-alone operation is developed in order to obtain voltage synchronization.

Special attention has been paid to the process of DFIG transition from the stand-alone operation mode to the grid operation mode using state feedback control. Solving the problem requires not only physical synchronization of stator and grid voltage, but also synchronization of the states of regulators which are separate for stand-alone and grid-connected operation modes. This problem does not occur in the classic cascaded control system but application of many resonant terms connected parallelly in classic cascaded control is troublesome when tuning to assure system stability.

The paper proposes a linear-quadratic regulator for power and torque control of DFIG operating under unbalanced voltage conditions. DFIG operation is shown in all potential modes: generator launch in the autonomous mode, generator synchronization and connection to an unbalanced grid. Control system targets in the grid-connected mode include reduction of electromagnetic torque ripples due to negative sequence influence and maintaining non-oscillatory stator reactive power. Other control targets are also identified (symmetrical stator currents, sinusoidal rotor currents, constant instantaneous powers) [15] but they are not analyzed in this paper because they concern stator or rotor current reference calculation and do not constitute a regulation problem [22]. The main objective of the paper is to obtain synchronization of stator voltage in the autonomous mode with grid voltage before grid connection. In classical stator voltage regulation with an inner current control loop this issue is quite trivial [16]. In the case of state feedback control of stator voltage, it requires (before the moment of connection) building the control signal of the controller carrying the work after connection

to the grid. Otherwise, once the grid connection operation controller is started with zero control signals, it may cause stator and rotor over-current even if stator and grid voltage are synchronized. In the steady state, both cascaded voltage control with the inner current control loop and state-feedback-based voltage controller may give similar results, when both methods involve oscillatory terms.

## 2. State controller

Although the electrical circuit model of the induction machine is non-linear, it is mostly considered linear with a varying parameter $\omega_m$. This is a minor simplification because the rotor speed varies very slowly in comparison with electrical state variables. This approach is also fundamental for using linear proportional-resonant controllers with decoupling terms in a cascade structure for DFIG [13]. The DFIG linear-quadratic regulator (LQR) has already been implemented using model linearization at a chosen operation point (particular rotor speed) [14]. This method provides for a convenient tuning procedure, especially when many resonant terms are present in the internal model of the control system, designed in order to provide disturbance suppression. The main drawback of building voltage-oriented control for a distorted grid with high harmonics is the tuning procedure based on a try-and-guess procedure, which can be very tiresome when there are many resonant terms. Moreover, stability is not guaranteed analytically. In contrast, LQR provides an elegant procedure for building the control system. However, its main drawback is that the DFIG mathematical model is non-stationary because some terms in the dynamic model depend on speed, which varies in time.

The state controller was designed in five steps. First, a plant model for autonomous operation was constructed and another one, without filtering capacitors, for the grid-operation mode. Second, the plant models had to be extended to include a disturbance dynamic model, which introduced auxiliary state variables. Two resonant terms were included in order to compensate for fundamental harmonic disturbances. Next, a novel method of plant model parameter fixing for linear-quadratic regulator design was used. Electromagnetic torque and reactive power tracking were the selected control targets in grid operation, thus adequate reference stator currents were calculated on the basis of instantaneous voltages and currents. Next, simultaneous synchronization of stator voltage with the grid and synchronization of the state controllers for stand-alone and grid operation was performed. Eventually, linear-quadratic optimization was applied in order to meet the requirements of fast stator current tracking in the case of grid-connected operation and of stator voltage disturbance rejection in the case of autonomous operation. A schematic diagram of the control structure is shown in Fig. 3.

**2.1. Plant models.** This paper uses the classical linear model of the induction machine (1–4). Its full description can be found in [17]. Additionally, equations (5–6) are calculated, describing voltage dynamics of capacitors connected to the stator side in

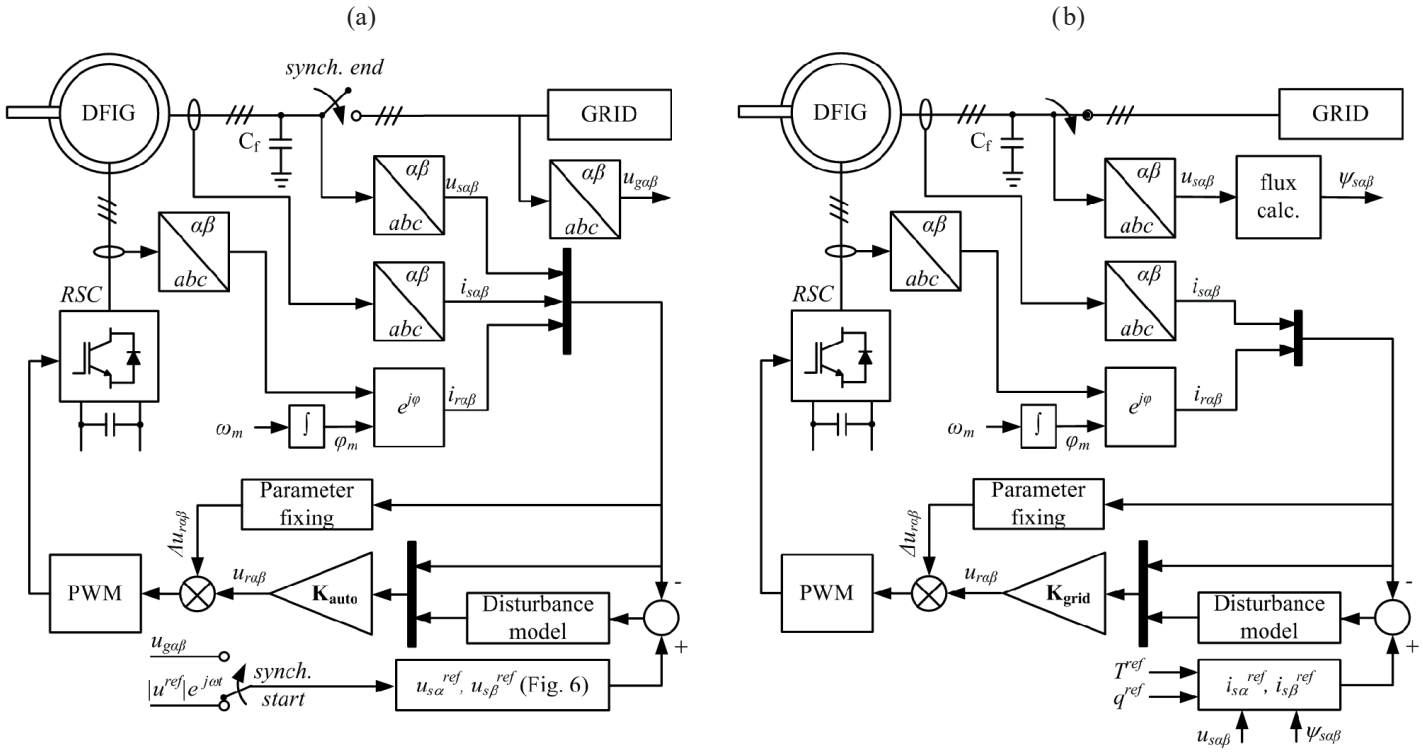


Fig. 3. Schemes of state feedback control structures for a) stand-alone mode before synchronization, b) grid-connected mode of DFIG

the stand-alone mode. Based on these six equations, state equations of the plant models which will be controlled are obtained.

$$u_{s\alpha} = R_s i_{s\alpha} + L_s \frac{di_{s\alpha}}{dt} + L_m \frac{di_{r\alpha}}{dt} \tag{1}$$

$$u_{s\beta} = R_s i_{s\beta} + L_s \frac{di_{s\beta}}{dt} + L_m \frac{di_{r\beta}}{dt} \tag{2}$$

$$u_{r\alpha} = R_r i_{r\alpha} + L_r \frac{di_{r\alpha}}{dt} + L_m \frac{di_{s\alpha}}{dt} - \omega_m \left(L_r i_{r\beta} + L_m i_{s\beta}\right) \tag{3}$$

$$u_{r\beta} = R_r i_{r\beta} + L_r \frac{di_{r\beta}}{dt} + L_m \frac{di_{s\beta}}{dt} - \omega_m \left(L_r i_{r\alpha} + L_m i_{s\alpha}\right) \tag{4}$$

$$\frac{du_{s\alpha}}{dt} = -C_f^{-1} i_{s\alpha} - \left(R_l C_f\right)^{-1} u_{s\alpha} \tag{5}$$

$$\frac{du_{s\beta}}{dt} = -C_f^{-1} i_{s\beta} - \left(R_l C_f\right)^{-1} u_{s\beta}. \tag{6}$$

**2.2. Grid operation.** In the control system for grid operation of DFIG, it is assumed that stator voltage is a disturbance, which will be compensated for by the internal model of the regulator. A plant model for grid operation that takes this into consideration is shown in (7). Four state variables are measurable, thus there is no need to use a state observer. Moreover, model (7) is controllable, thus system dynamics can be freely adjusted with full-state feedback.

$$\frac{d}{dt} = \begin{bmatrix} i_{s\alpha} \\ i_{s\beta} \\ i_{r\alpha} \\ i_{r\beta} \end{bmatrix} = \boldsymbol{A_{grid}} \begin{bmatrix} i_{s\alpha} \\ i_{s\beta} \\ i_{r\alpha} \\ i_{r\beta} \end{bmatrix} + \boldsymbol{B_{grid}} \begin{bmatrix} u_{r\alpha} \\ u_{r\beta} \end{bmatrix}$$

$$\boldsymbol{A_{grid}} = \left(\sigma L_s L_r\right)^{-1} \begin{bmatrix} -R_s L_r & \omega_m L_m^2 & R_r L_m & \omega_m L_r L_m \\ -\omega_m L_m^2 & -R_s L_r & -\omega_m L_r L_m & R_r L_m \\ R_s L_m & -\omega_m L_s L_m & R_r L_s & -\omega_m L_r L_s \\ \omega_m L_s L_m & R_s L_m & \omega_m L_r L_s & R_r L_s \end{bmatrix} \tag{7}$$

$$\boldsymbol{B_{grid}} = \left(\sigma L_s L_r\right)^{-1} \begin{bmatrix} L_r & 0 & -L_m & 0 \\ 0 & L_r & 0 & -L_m \\ -L_m & 0 & L_s & 0 \\ 0 & -L_m & 0 & L_s \end{bmatrix}.$$

**2.3. Stand-alone operation.** Autonomous operation requires extending the plant state vector to include stator voltages, which are state variables emerging due to the operation of stator-connected filtering capacitors. Load current is treated as a disturbance in the autonomous DFIG model, similarly to other stand-alone systems such as inverters equipped with LC filters generating sinusoidal voltage waveforms. Resonant terms compensate for load current influence despite loading conditions, provided that the load is linear. In the paper, an autonomous DFIG under no-load conditions is modeled as this is the most difficult situation due to the lowest damping in the system.

$$\frac{d}{dt} = \begin{bmatrix} i_{s\alpha} \\ i_{s\beta} \\ i_{r\alpha} \\ i_{r\beta} \\ u_{s\beta} \\ u_{s\beta} \end{bmatrix} = \boldsymbol{A_{auto}} \begin{bmatrix} i_{s\alpha} \\ i_{s\beta} \\ i_{r\alpha} \\ i_{r\beta} \\ u_{s\beta} \\ u_{s\beta} \end{bmatrix} + \boldsymbol{B_{auto}} \begin{bmatrix} u_{r\alpha} \\ u_{r\beta} \end{bmatrix}$$

$$\boldsymbol{A_{auto}} = \left(\sigma L_s L_r\right)^{-1} \begin{bmatrix} -R_s L_r & \omega_m L_m^2 & R_r L_m & \omega_m L_r L_m & L_r & 0 \\ -\omega_m L_m^2 & -R_s L_r & -\omega_m L_r L_m & R_r L_m & 0 & L_r \\ R_s L_m & -\omega_m L_s L_m & R_r L_s & -\omega_m L_r L_s & L_m & 0 \\ \omega_m L_s L_m & R_s L_m & \omega_m L_r L_s & R_r L_s & 0 & L_m \\ -C_f^{-1}(\sigma L_s L_r) & 0 & 0 & 0 & 0 & 0 \\ 0 & -C_f^{-1}(\sigma L_s L_r) & 0 & 0 & 0 & 0 \end{bmatrix} \tag{8}$$

$$\boldsymbol{B_{auto}} = \left(\sigma L_s L_r\right)^{-1} \begin{bmatrix} L_r & 0 & -L_m & 0 \\ 0 & L_r & 0 & -L_m \\ -L_m & 0 & L_s & 0 \\ 0 & -L_m & 0 & L_s \\ 0 & 0 & 0 & 0 \\ 0 & 0 & 0 & 0 \end{bmatrix}.$$

Moreover, this mode is used here only for synchronization of stator voltage with grid voltage and not for load supply. Influence of the load current on stator voltage is a broad topic, related not only to unbalance and harmonics but also to over-current protections. The problem of state feedback control synthesis during load current unbalance and harmonics has already been solved in [26]. Model (8), describing stand-alone DFIG, is also controllable but it now has 6 state variables.

Stability of the closed-loop DFIG system under varying parameters can be evaluated by observing the trajectories of its eigenvalues. Feedback gain has been designed using one set of plant parameters, whereas the eigenvalues trajectories of the closed-loop system have been calculated for changing the machine speed. Variability of resistances has a minor impact on damping of the closed-loop system. Variability of rotor speed (Fig. 4) has a much more significant impact on the model dynamics despite the feedback loop with LQR.

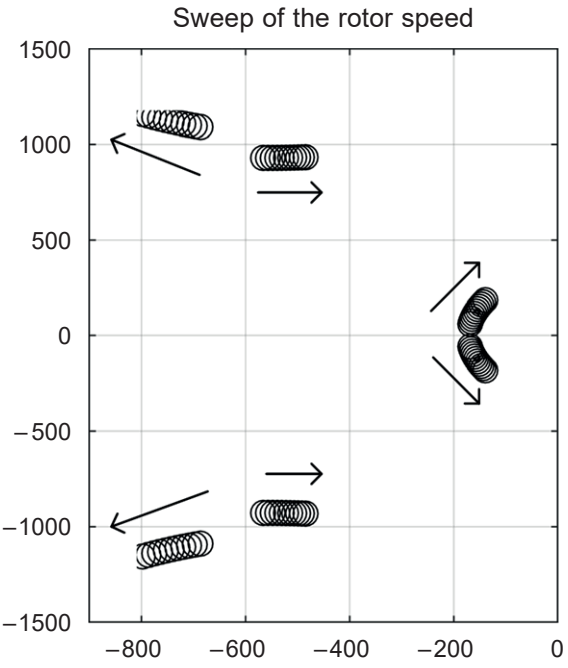


Fig. 4. Eigenvalues trajectories under varying model parameters and constant-gain state feedback control: a) sweep of rotor angular speed in the range of (0.7 $\omega_s$, 1.3 $\omega_s$)

**2.4. Auxiliary states.** A closed-loop system rejects disturbances if the plant model is augmented by extra dynamic terms representing disturbances dynamics. In the case of the model built within the $\alpha\beta$ frame, additional oscillatory terms are created using the following pairs of variables: $x_{\alpha 1}$–$x_{\alpha 2}$, $x_{\beta 1}$–$x_{\beta 2}$ for each axis, respectively, and the plant models (for autonomous operation (9a) and grid operation (9b)) are augmented by two resonant terms, each with resonant pulsation $\omega_s$ equal to the grid voltage pulsation.

**2.5. Model parameter fixing.** Thus created augmented models (9a) and (9b) are linear but still dependent on the rotor speed due to basic state matrices $\boldsymbol{A}_{auto}$ (8) and $\boldsymbol{A}_{grid}$ (7). Therefore, the actual plant changes under variable-speed operation. Modern control theory presents two main ways of handling linear parameter-varying systems.

$$\frac{d}{dt}\begin{bmatrix} i_{s\alpha} \\ i_{s\beta} \\ i_{r\alpha} \\ i_{r\beta} \\ u_{s\beta} \\ u_{s\beta} \\ x_{\alpha 1} \\ x_{\alpha 2} \\ x_{\beta 1} \\ x_{\beta 2} \end{bmatrix} = \begin{bmatrix} \boldsymbol{A}_{auto} & \mathbf{0}^{6\times 4} \\ \begin{bmatrix} \mathbf{0}^{2\times 4} & \mathbf{0}^{2\times 2} \\ \mathbf{0}^{2\times 4} & \mathbf{1}^{2\times 2} \end{bmatrix} & \begin{bmatrix} \mathbf{0}^{2\times 2} & \mathbf{1}^{2\times 2} \\ -\omega_s \mathbf{1}^{2\times 2} & \mathbf{0}^{2\times 2} \end{bmatrix} \end{bmatrix} \begin{bmatrix} i_{s\alpha} \\ i_{s\beta} \\ i_{r\alpha} \\ i_{r\beta} \\ u_{s\beta} \\ u_{s\beta} \\ x_{\alpha 1} \\ x_{\alpha 2} \\ x_{\beta 1} \\ x_{\beta 2} \end{bmatrix} + \begin{bmatrix} \boldsymbol{B}_{auto} \\ \mathbf{0}^{4\times 2} \end{bmatrix} \begin{bmatrix} u_{r\alpha} \\ u_{r\beta} \end{bmatrix} \tag{9a}$$

$$\frac{d}{dt}\begin{bmatrix} i_{s\alpha} \\ i_{s\beta} \\ i_{r\alpha} \\ i_{r\beta} \\ x_{\alpha 1} \\ x_{\alpha 2} \\ x_{\beta 1} \\ x_{\beta 2} \end{bmatrix} = \begin{bmatrix} \boldsymbol{A}_{grid} & \mathbf{0}^{4\times 4} \\ \begin{bmatrix} \mathbf{0}^{2\times 2} & \mathbf{0}^{2\times 2} \\ \mathbf{1}^{2\times 2} & \mathbf{0}^{2\times 2} \end{bmatrix} & \begin{bmatrix} \mathbf{0}^{2\times 2} & \mathbf{1}^{2\times 2} \\ -\omega_s \mathbf{1}^{2\times 2} & \mathbf{0}^{2\times 2} \end{bmatrix} \end{bmatrix} \begin{bmatrix} i_{s\alpha} \\ i_{s\beta} \\ i_{r\alpha} \\ i_{r\beta} \\ x_{\alpha 1} \\ x_{\alpha 2} \\ x_{\beta 1} \\ x_{\beta 2} \end{bmatrix} + \begin{bmatrix} \boldsymbol{B}_{grid} \\ \mathbf{0}^{2\times 2} \end{bmatrix} \begin{bmatrix} u_{r\alpha} \\ u_{r\beta} \end{bmatrix} \tag{9b}$$

$\mathbf{1}^{n\times n}$ – *matrix with ones on the diagonal*
$\mathbf{0}^{m\times n}$ – *matrix of zeros.*

One, suitable for systems with parameters that change only slightly, is robust control, described in detail in [18]. In this method, controllers are tuned in the nominal operation point and they are meant to react to parameter changes as little as possible. Another method is designed for systems with parameters that change significantly but can be measured and utilized to adapt the controller during system operation. Gain-scheduled controllers are tuned in many operation points and controller gain is approximated across varying parameter [19]. Tuning of gain-scheduled controllers may be tiresome due to many tuning procedure calls. Moreover, simple linear approximations of the feedback gains obtained are not always satisfactory.

Plant parameter fixing is done indirectly within the classical decoupled control of DFIG because varying rotor speed is present only in the cross coupling terms of the DFIG model. Decoupling instantly fixes parameters of the controlled plant. It is proposed to use a parameter fixing feedback loop which has a formula similar to decoupling terms in the classical field-oriented control, except that the proposed parameter fixing loop

does not fully decouple state variables. Instead, it makes this coupling speed invariant. This is not a problem for state feedback control because this type of control takes into consideration the full state of the plant and not only the state of one control path (either $\alpha$ or $\beta$ here) as is the case in the cascaded control structure. Thus, the coupling parameters between the $\alpha\beta$ axes may remain constant.

State matrices of models (7) and (8) are decomposed into two separate matrices each, one that is rotor-speed-independent and another dependent on rotor speed, as shown in (10). By splitting the control action into two state-feedback loops (11) and finding such gain $\tilde{\boldsymbol{K}}(\omega_m)$ that (13) is true, the closed-loop system (12) is reduced to parameter-constant model (14).

$$\dot{\boldsymbol{x}} = \left(\bar{\boldsymbol{A}} + \tilde{\boldsymbol{A}}(\omega_m)\right)\boldsymbol{x} + \boldsymbol{B}\boldsymbol{u} \tag{10}$$

$$\boldsymbol{u} = \bar{\boldsymbol{u}} + \tilde{\boldsymbol{u}}(\omega_m) = -\bar{\boldsymbol{K}}\boldsymbol{x} - \tilde{\boldsymbol{K}}(\omega_m)\boldsymbol{x} \tag{11}$$

$$\dot{\boldsymbol{x}} = \left(\bar{\boldsymbol{A}} - \boldsymbol{B}\bar{\boldsymbol{K}}\right)\boldsymbol{x} + \left(\tilde{\boldsymbol{A}}(\omega_m) - \boldsymbol{B}\tilde{\boldsymbol{K}}(\omega_m)\right)\boldsymbol{x} \tag{12}$$

$$\left(\tilde{\boldsymbol{A}}(\omega_m) - \boldsymbol{B}\tilde{\boldsymbol{K}}(\omega_m)\right) = \boldsymbol{0} \tag{13}$$

$$\dot{\boldsymbol{x}} = \left(\bar{\boldsymbol{A}} - \boldsymbol{B}\bar{\boldsymbol{K}}\right)\boldsymbol{x}. \tag{14}$$

Due to the special structure of the state matrix of the DFIG model, (13) can be solved while rotor-speed-dependent control signal $\tilde{\boldsymbol{u}}(\omega_m)$ (15) fixes the parameters of the plant model. After implementing this internal parameter fixing loop, classical state feedback control methods can be applied for this linear time-invariant model.

$$\tilde{\boldsymbol{u}}(\omega_m) = \begin{bmatrix} (\omega_s - \omega_m)L_m i_{s\beta} + (\omega_s - \omega_m)L_m i_{r\beta} \\ -(\omega_s - \omega_m)L_m i_{s\alpha} - (\omega_s - \omega_m)L_m i_{r\alpha} \end{bmatrix}. \tag{15}$$

A system with the presented inner feedback loop can be controlled using LQR without other adaptation mechanisms because the impact of changing rotor speed is compensated for by the inner feedback loop. It can be seen that this feedback loop (15) is very similar to the decoupling terms used in FOC and VOC methods. The difference is that cross couplings are not cancelled but simply rendered rotor-speed-invariant. This additional parameter fixing signal converges to 0 when rotor speed goes to synchronous speed. The control signal produced by the parameter fixing loop is small in comparison to the signal produced by main state feedback. When the auxiliary feedback loop is applied into the DFIG control scheme, the eigenvalues of the closed-loop system remain constant despite changes in rotor speed.

**2.6. Reference calculation.** The state feedback controller provides for reference tracking and disturbance rejection but precise calculation of the reference signals is equally important. The references for an autonomous DFIG are stator voltages. Before connecting DFIG to the grid, stator voltage should be smoothly synchronized to the grid voltage in order not to cause stator current swell during the connection. In case of small voltage unbalances, stator voltage can be synchronized only to the positive sequence of grid voltage. When the grid is highly unbalanced, both positive and negative sequences of stator voltage should be synchronized [20].

DFIG synchronization with an unbalanced grid can be performed using a tracking system based on a second-order general integrator (SOGI), presented in Fig. 5. SOGI amplifies a selected frequency of the input signal and attenuates others. A simple feedback loop comparing a reference signal with the output of SOGI creates the tracking system of a selected spectral component of the reference signal. Using the presented system as the reference filter of the stator voltage reference signal, it is possible to smoothly synchronize DFIG voltage with the unbalanced grid. Initially, reference is given arbitrarily symmetrically, and in some instant $t_o$, depending on the superior control, the reference changes to grid voltage signal $u_{g\alpha}$, $u_{g\beta}$. Finally, reference stator voltage $u_{s\alpha}^{ref}$, $u_{s\beta}^{ref}$ equals the grid voltage, and assuming that SOGI filter dynamics are slower than state feedback control, the generated stator voltage $u_{s\alpha}$, $u_{s\beta}$ is synchronized simultaneously with grid voltage $u_{g\alpha}$, $u_{g\beta}$.

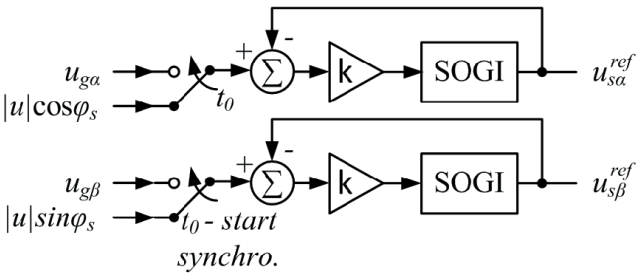


Fig. 5. Voltage synchronization of DFIG with unbalanced grid voltage

In the grid operation, the electromagnetic torque and reactive power are the reference signals provided by a superior controller (e.g. MPPT, the reactive power management system dependent on grid codes). They have to be translated into the stator current references within the $\alpha\beta$ reference frame [21], which are used for current control with state feedback. Equations (16) and (17) can serve to obtain stator current which will produce the commanded electromagnetic torque and reactive power of grid-connected DFIG [23].

$$i_{s\alpha}^{ref} = \frac{2\left(T^{ref}u_{s\alpha} + q^{ref}p\psi_{s\alpha}\right)}{3p\left(u_{s\alpha}\psi_{s\beta} - u_{s\beta}\psi_{s\alpha}\right)} \tag{16}$$

$$i_{s\beta}^{ref} = \frac{2\left(T^{ref}u_{s\beta} + q^{ref}p\psi_{s\beta}\right)}{3p\left(u_{s\alpha}\psi_{s\beta} - u_{s\beta}\psi_{s\alpha}\right)}. \tag{17}$$

Stator flux occurring in (16) and (17) is usually estimated by integrating stator voltage and filtration in order to eliminate stator voltage measurement offsets and noises [22].

**2.7. Linear-quadratic regulator.** Dynamics of controllable linear systems can be adjusted with pole placement in single-input single-output systems and with eigenstructure assignment in multiple-input multiple-output systems. The choice of adequate eigenvalues and eigenvectors to meet technical requirements (rising time, settling time, overshot) is in general complicated and non-trivial. Optimization methods are frequently used to obtain feedback gains. Linear-quadratic optimization, which minimizes function (18), representing signal energy in the controlled system, is often used to tune state controllers.

$$J = \int_0^\infty \boldsymbol{x}^T(t)\boldsymbol{Q}\boldsymbol{x}(t) + \boldsymbol{u}^T(t)\boldsymbol{R}\boldsymbol{u}(t)dt. \tag{18}$$

Although the choice of the eigenvalue structure is eliminated using LQR, penalty matrices ($\boldsymbol{Q}$, $\boldsymbol{R}$) have to be selected. Nonetheless, the linear-quadratic regulator is easier to tune than the state controller with eigenvalue assignment due to intuitive physical interpretation of goal function (18). Iterative tuning of LQR by means of the trial-and-error method is usually used but lately some automatic methods, such as particle swarm optimization, are successfully used in the tuning procedure [25]. In the paper, penalty matrices are chosen by means of trial-and-error tuning, and for small systems they are effective enough. Appendix A shows the chosen $\boldsymbol{Q}$ and $\boldsymbol{R}$ penalty matrices. The control action extended by resonant terms for stand-alone operation is described by (19, 20), whereas control action extended by resonant terms for a grid-connected system is described by (21, 22). Individual gains $k$ for each state variable are provided in Appendix A.

$$\begin{aligned} u_{r\alpha} = &-k_{\alpha1}i_{s\alpha} - k_{\alpha2}i_{s\beta} - k_{\alpha3}i_{r\alpha} - k_{\alpha4}i_{r\beta} - k_{\alpha5}u_{s\alpha} - \\ &- k_{\alpha6}u_{s\beta} - k_{\alpha7}x_{\alpha1} - k_{\alpha8}x_{\alpha2} - k_{\alpha9}x_{\beta1} - k_{\alpha10}x_{\beta2} \end{aligned} \tag{19}$$

$$\begin{aligned} u_{r\beta} = &-k_{\beta1}i_{s\alpha} - k_{\beta2}i_{s\beta} - k_{\beta3}i_{r\alpha} - k_{\beta4}i_{r\beta} - k_{\beta5}u_{s\alpha} - \\ &- k_{\beta6}u_{s\beta} - k_{\beta7}x_{\alpha1} - k_{\beta8}x_{\alpha2} - k_{\beta9}x_{\beta1} - k_{\beta10}x_{\beta2} \end{aligned} \tag{20}$$

$$\begin{aligned} u_{r\alpha} = &-k_{\alpha1}i_{s\alpha} - k_{\alpha2}i_{s\beta} - k_{\alpha3}i_{r\alpha} - k_{\alpha4}i_{r\beta} - k_{\alpha5}x_{\alpha1} - \\ &- k_{\alpha6}x_{\alpha2} - k_{\alpha7}x_{\beta1} - k_{\alpha8}x_{\beta2} \end{aligned} \tag{21}$$

$$\begin{aligned} u_{r\beta} = &-k_{\beta1}i_{s\alpha} - k_{\beta2}i_{s\beta} - k_{\beta3}i_{r\alpha} - k_{\beta4}i_{r\beta} - k_{\beta5}x_{\alpha1} - \\ &- k_{\beta6}x_{\alpha2} - k_{\beta7}x_{\beta1} - k_{\beta8}x_{\beta2}. \end{aligned} \tag{22}$$

The LQR structure cannot be divided into separate control feedback loops for individual variables, in contrast to the situation in the cascade control scheme. A common current control loop for both operation modes in the cascade structure makes connection to the grid smooth because the current controller keeps rotor voltage invariant during the connection. But let us assume that just before connection to the grid the generator was not loaded. Then, if the stator and rotor voltage keep their amplitude and frequency during changing operation modes, the connection is made without the stator current transient.

The LQR structures for the autonomous and grid-operation modes are separate (resonant terms are connected to different signals; the numbers of system state variables are also different). Therefore, in order to effect smooth switching between operation modes, these two controllers should be synchronized at the time of stator and grid voltage synchronization. The regulator synchronization algorithm is presented in Fig. 6. The difference between the output signal of the autonomous-operation state-controller and the output signal of the grid-operation state-controller is enhanced by a proportional-resonant P-R regulator and fed to the resonant terms of the grid-operation state controller. Figure 7 and Fig. 8 show stator voltage, stator current, electromagnetic torque and stator powers during the synchronization of stator voltage with the grid. If there is no synchronization of the controllers – this

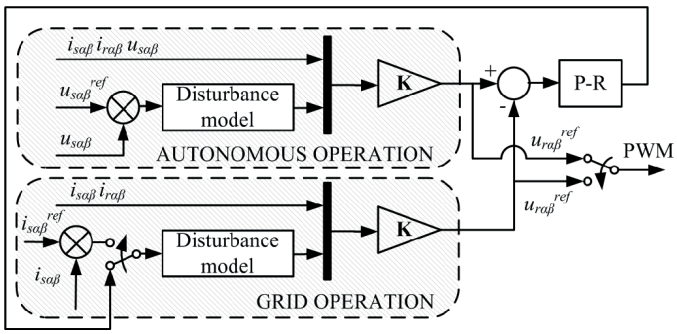


Fig. 6. Synchronization of state controllers with an additional feedback loop and proportional-resonant controller P-R, which is switched on during stator voltage synchronization with the grid

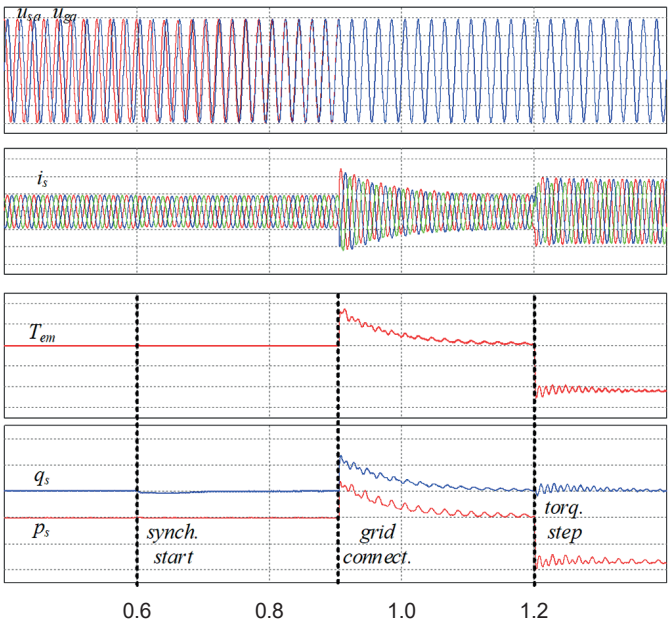


Fig. 7. Synchronization of stator voltage with the grid without simultaneous synchronization of state controllers

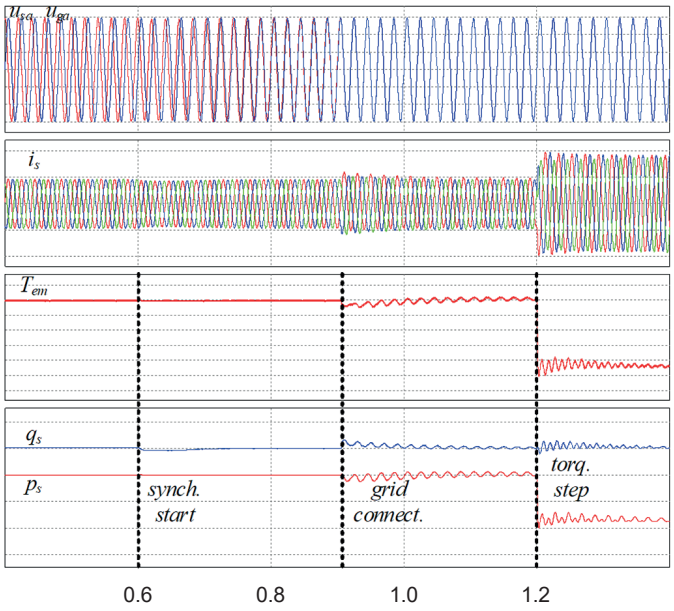


Fig. 8. Synchronization of stator voltage with the grid with synchronization of state controllers

situation is shown in Fig. 7 – there is a stator current swell during the connection, which produces torque and power ripples after the connection.

## 3. Experimental verification under unbalanced grid voltage conditions

The presented system was verified in a laboratory rig with a 7.5 kW DFIG driven by a speed-controlled DC machine. DFIG parameters are shown in Table 1 in Appendix B. The control algorithm was implemented in a Texas Instruments digital signal controller TMS320F28335 and all experimental results were acquired using a Yokogawa ScopeCorder DL850E. Autonomous operation of DFIG was performed in order to synchronize the generator with an unbalanced grid. DFIG was connected to filtering capacitors in the autonomous mode, which also provided a fraction of the reactive power required for magnetization of the machine. The unbalanced grid was created with a multi-tap transformer (voltage unbalanced factor that is defined in [26] stood at 21%). DFIG was connected to the grid following the synchronization procedure.

Figures 9–11 present reference torque and reactive power steps under unbalanced voltage conditions. Unfortunately, in the laboratory grid there is a visible content of high harmonics, which slightly deforms the shape of stator currents. However, despite significant asymmetry of the grid voltage, torque and stator reactive power ripples have been eliminated. It is not possible to reach full rated torque due to the construction of the slip ring machine used in the laboratory, which is designed for magnetization from the stator side, and the rotor rated current is lower than the stator rated current. When magnetization is provided from the rotor side, as typically in DFIG systems with back-to-back power converters, the rotor current active component responsible for torque production is significantly lower than the rated value.

Figure 9 shows step change of the reference torque from zero to half of the rated value. The rotor current reaches the rated value. The step response is rapid due to implementation of the input model. Some small oscillations of indirectly controlled variables ($T_{em}$, $q_s$) occur at the beginning of the step because oscillatory terms require some time to fully eliminate the steady state error of the state feedback controller. Oscillations of the $p_s$ power component are significant despite a relatively low voltage asymmetry factor but it is impossible to eliminate torque and active power oscillations at the same time, and elimination of $p_s$ power components is not the goal of this paper. Figure 10 shows stator current tracking (four bottom waveforms on the oscillograms are actual and reference $\alpha\beta$ components of the stator current) following a step in

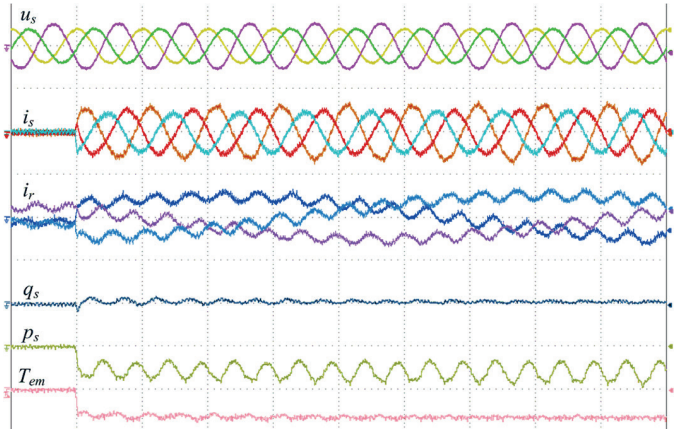


Fig. 9. Step in reference torque from 0 Nm to –22.5 Nm under 0 var stator reactive power; the following are shown: phase stator voltages $u_s$, stator currents $i_s$, rotor currents $i_r$, stator active power $p_s$, stator reactive power $q_s$ and torque $T_{em}$

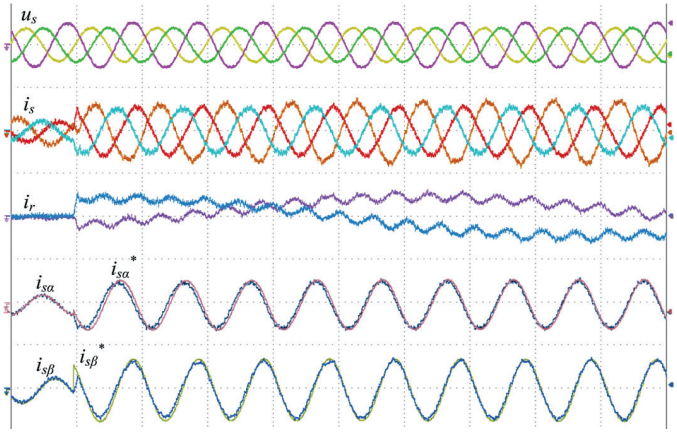


Fig. 10. Step in reference torque from 0 Nm to –22.5 Nm under 1500 var stator reactive power; the following are shown: phase stator voltages $u_s$, stator currents $i_s$, rotor currents $i_r$, $\alpha$ and $\beta$ components of reference stator current $i_{s\alpha}^*$ $i_{s\beta}^*$, $\alpha$ and $\beta$ components of stator current $i_{s\alpha}$ $i_{s\beta}$

the reference electromagnetic torque under 1500 var of the $q_s$ power component.

Figure 11 shows the step in the reference $q_s$ component of stator power from zero to 3 kvar at fixed reference torque of the machine equal to half of the rated value. Thus obtained transients dynamics and elimination of controlled variables oscillations are analogical to the case of the reference torque step

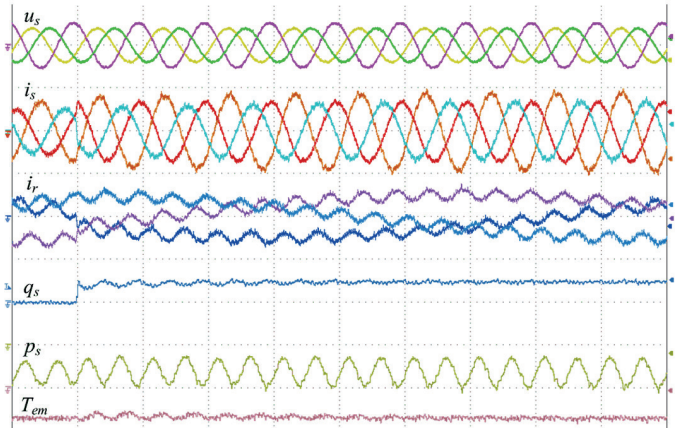


Fig. 11. Step in reference reactive power from 0 var to 3000 var under –22.5 Nm torque; the following are shown: phase stator voltages $u_s$, stator currents $i_s$, rotor currents $i_r$, stator active power $p_s$, stator reactive power $q_s$ and torque $T_{em}$

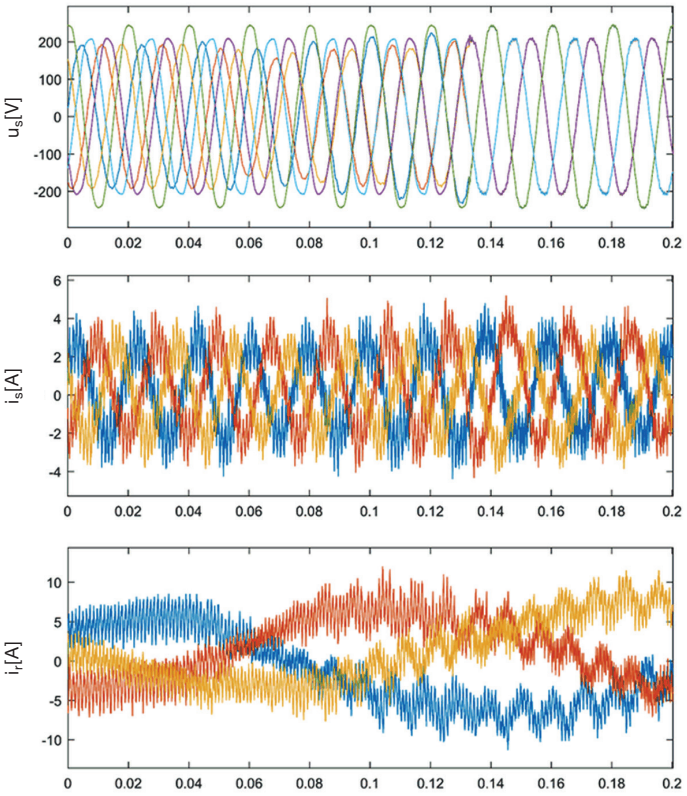


Fig. 12. Synchronization and connection to the grid of the DFIG system without load. The following are shown: stator voltages $u_s$, grid voltages $u_s$, stator currents $i_s$ and rotor currents $i_r$

changes. The reference torque step made, shown in Fig. 9, is an extreme situation because under normal operation conditions the reference power changes gradually, according to the MPPT algorithm.

Figure 12 presents synchronization and connection of DFIG to an unbalanced grid without load. Significant swells were not observed in the stator current. Before DFIG connection to the grid, stator and grid voltages were synchronized using the presented SOGI tracker (Fig. 5). State controllers for autonomous and grid operation were also synchronized.

This issue has been explained in subsection 2.6, where comparative simulation results with and without synchronization of state controllers have been shown. Synchronization of voltages within the stationary frame renders both the decomposition of symmetrical sequences and the PLL synchronization loop obsolete.

In this paper, the methodology of state feedback controllers synchronization was verified only for the positive and negative sequence of fundamental harmonics. It seems that resonant terms for higher harmonics do not need to be synchronized because the content of harmonics is negligible in comparison with the negative sequence.

## 4. Conclusions

The main goal of the paper, i.e. state feedback control application to the stand-alone and grid-connected doubly fed induction generator, has been achieved. Although state feedback control is known in automatic control, using it for the doubly fed induction generator requires solving two main problems. The first one is to adapt the controller to the operation point of the control plant with varying parameters. The second issue is to find the initial conditions of the controller operating after connection to the grid. The first problem has been solved by proposing an additional loop creating a speed invariant DFIG model. The second problem has been solved by means of controller output synchronization during transition from stand-alone to grid-connected operation.

The experiment conducted shows satisfying performance of the generator system in the grid-connected operation mode and smooth connection of the autonomous DFIG to the grid. The simplification made in the DFIG model in this paper, i.e. that rotor speed is constant in the transients of stator and rotor current, can be justified for a vast group of DFIG applications (e.g. wind turbines). The mechanical time constant is 1–2 orders of magnitude larger than the electrical time constant for wind energy conversion systems. This paper shows a promising perspective for state controller application for doubly fed induction generator control, in spite of rare use of state controllers for induction machines nowadays. The manner of model parameters fixing is valid also for the cage induction machine and can be used in its motor and generator control.

**Acknowledgements.** The work is supported by the statutory funds of the Faculty of Electrical Engineering, Warsaw University of Technology.

## References

[1] R. Cardenas, R. Pena, S. Alepuz, and G. Asher, "Overview of control systems for the operation of DFIGs in wind energy applications", *IEEE Trans. Ind. Electron.*, vol. 60, no. 7, pp. 2776–2798, July 2013.

[2] A. Bocquel and J. Janning, "Analysis of a 300 MW Variable Speed Drive for Pump-Storage Plant Applications", *Eur. Conf. Power Electron. Appl. – EPE'05*, pp. 1–10, Dresden, 2005.

[3] N. Mendis, K.M. Muttaqi, S. Perera, and S. Kamalasadan, "An Effective Power Management Strategy for a Wind – Diesel – Hydrogen-Based Remote Area Power Supply System to Meet Fluctuating Demands Under Generation Uncertainty", *IEEE Trans Ind Appl*, vol. 51, no. 2, pp. 1228–1238, March-April 2015.

[4] R. Peña, R. Cárdenas, J. Proboste, J. Clare, and G. Asher, "Wind-Diesel Generation Using Doubly Fed Induction Machines", *IEEE Trans. Energy Conv.*, vol. 23, no. 1, pp. 202–214, March 2008.

[5] L. Wang, J-Y. Yu, and Y-T. Chen, "Dynamic stability improvement of an integrated offshore wind and marine-current farm using a flywheel energy-storage system", *IET Renew. Power Gener.,* vol. 5, no. 5, pp. 387–396, Sept. 2011.

[6] H. Camblong, I.M. de Alegria, M. Rodriguez, and G. Abad, "Experimental evaluation of wind turbines maximum power point tracking controllers", *Energy Convers. Manag.*, vol. 47, no. 18–19, pp. 2846–2858, Nov. 2006.

[7] Xu Lie and Yi Wang,"Dynamic Modeling and Control of DFIG-Based Wind Turbines Under Unbalanced Network Conditions", *IEEE Trans. on Power Systems*, vol. 22, no. 1, pp. 314–323, Feb. 2007.

[8] J. Hu; J. Zhu; and D.G. Dorrell, "Predictive Direct Power Control of Doubly Fed Induction Generators Under Unbalanced Grid Voltage Conditions for Power Quality Improvement," *IEEE Trans. on Sust. Energy*, vol. 6, no. 3, pp. 943–950, July 2015.

[9] L. Shang and J. Hu, "Sliding-Mode-Based Direct Power Control of Grid-Connected Wind-Turbine-Driven Doubly Fed Induction Generators Under Unbalanced Grid Voltage Conditions", *IEEE Trans. Energy Conv.*, vol. 27, no. 2, pp. 362–373, June 2012.

[10] X. Lie and P. Cartwright, "Direct Active and Reactive Power Control of DFIG for Wind Energy Generation", *IEEE Trans Energy Conv.*, vol. 21, no. 3, pp. 750–758, Sept. 2006.

[11] D. Santos-Martin, J.L. Rodriguez-Amenedo, and S. Arnalte", Direct Power Control Applied to Doubly Fed Induction Generator Under Unbalanced Grid Voltage Conditions", *IEEE Trans Power Electron.,* vol. 23, no. 5, pp. 2328–2336, Sept. 2008.

[12] G. Abad, M.A. Rodriguez, G. Iwanski, and J. Poza, "Direct Power Control of Doubly-Fed-Induction- Generator-Based Wind Turbines Under Unbalanced Grid Voltage", *IEEE Trans. Power Electron.,* vol. 25, no. 2, pp. 442–452, Feb. 2010.

[13] J. Hu, Y. He, L. Xu, and B.W. Williams, "Improved control of DFIG systems during network unbalance using PI-R current regulators", *IEEE Trans. Ind. Electron.,* vol. 56, no. 2, pp. 439–451, Feb. 2009.

[14] B. Kedjar and K. Al-Haddad, "LQR with Integral Action Applied to a Wind Energy Conversion System Based on Doubly Fed Induction Generator", *IEEE 24th Can. Conf. Electr. Comput. Eng.*, pp. 717–722, Niagara Falls, Canada, 8–11 May 2011.

[15] L. Shang, D. Sun, and J. Hu, "Sliding-Mode-Based Direct Power Control of Grid-Connected Voltage-Sourced Inverters under Unbalanced Network Conditions", *IET Power Electron*., vol. 4, no. 5, pp. 570–579, May 2011.

[16] G. Iwanski and W. Koczara, "DFIG-Based Power Generation System with UPS Function for Variable-Speed Applications", *IEEE Trans. Ind. Electron.,* vol. 55, no. 8, pp. 3047–3054, Aug. 2008.

[17] G. Abad, J. López, M.A. Rodríguez, L. Marroyo, and G. Iwanski, "Doubly Fed Induction Machine: Modeling and Control for Wind Energy Generation", Hoboken, NJ, USA: John Wiley & Sons, Inc.; 2011.

[18] K. Zhou and J. Doyle, K. Glover, "Robust and Optimal Control", Prentice Hall; 1996.

[19] W.J. Rugh and J.S. Shamma, "Research on gain scheduling", Automatica, vol. 36, no. 10, pp. 1401–1425, Oct. 2000.

[20] S.Z. Chen, N.C. Cheung, Y. Zhang, M. Zhang, and X.M. Tang, "Improved grid synchronization control of doubly fed induction generator under unbalanced grid voltage", *IEEE Trans Energy Convers,* vol. 26, no. 3, pp. 799–810, Sept. 2011.

[21] G. Iwanski, P. Pura, and T. Luszczyk, "Properties and control of variable speed doubly fed induction generator", *10th Int. Conf. Ecol. Veh. Renew. Energies*, pp. 1–8, Monte carlo, Monaco, 31March – 2April 2015.

[22] G. Iwanski, T. Łuszczyk, and P. Pura, "Indirect Torque and Stator Reactive Power Control of Doubly Fed Induction Machine Connected to Unbalanced Power Network", *IEEE Trans Energy Convers,* vol. 31, no. 3, pp. 1202–1211, 2016.

[23] P. Rodríguez, A. Luna, I. Candela, R. Mujal, R. Teodorescu, and F. Blaabjerg, "Multiresonant Frequency-Locked Loop for Grid Synchronization of Power Converters under Distorted Grid Conditions", *IEEE Trans Ind Electron,* vol. 58, no. 1, pp.127–138, Jan. 2011.

[24] B. Ufnalski, A. Kaszewski, and L.M. Grzesiak, "Particle Swarm Optimization of the Multioscillatory LQR for a Three-Phase Four-Wire Voltage-Source Inverter with an LC Output Filter", *IEEE Trans Ind Electron*, vol. 62, no. 1, pp. 484–493, Jan. 2015.

[25] P. Pillay and M. Manyage, "Definitions of voltage unbalance", *IEEE Power Eng. Rev. Mag.*, vol. 5, pp. 50–51, May 2001.

[26] M. Szypulski and G. Iwanski, "Sensorless State Control of Stand-Alone Doubly Fed Induction Generator Supplying Nonlinear and Unbalanced Loads," in *IEEE Transactions on Energy Conversion*, vol. 31, no. 4, pp. 1530–1538, Dec. 2016.

## Appendix A.

$$\boldsymbol{Q}_{auto} = diag\left(\left[0.0013,\ 0.0013,\ 0.0016,\ 0.0016,\ 6.92\cdot 10^{-6},\ 6.92\cdot 10^{-6},\ 5\cdot 10^{5},\ 5\cdot 10^{5},\ 5.07,\ 5.07\right]\right)$$

$$\boldsymbol{R}_{auto} = diag\left(\left[3.35\cdot 10^{-6},\ 3.35\cdot 10^{-6}\right]\right)$$

$$\boldsymbol{Q}_{grid} = diag\left(\left[0.013,\ 0.013,\ 0.0016,\ 0.0016,\ 5\cdot 10^{5},\ 5\cdot 10^{5},\ 5.07,\ 5.07\right]\right)$$

$$\boldsymbol{R}_{grid} = diag\left(\left[3.35\cdot 10^{-6},\ 3.35\cdot 10^{-6}\right]\right).$$

Gains obtained for stand-alone operation:

$$k_{\alpha 1} = -2.4721487907177195$$
$$k_{\alpha 2} = -26.199722024284885$$
$$k_{\alpha 3} = 33.100006713126909$$
$$k_{\alpha 4} = -24.910814027023473$$

$k_{\alpha 5} = 0.82350178697695897$
$k_{\alpha 6} = 0.08449827097236072$
$k_{\alpha 7} = -13642.429823061711$
$k_{\alpha 8} = -1460.6433991669999$
$k_{\alpha 9} = -191.46916492232302$
$k_{\alpha 10} = -20.499879868614062$
$k_{\beta 1} = 26.199722023292015$
$k_{\beta 2} = -2.4721487911581304$
$k_{\beta 3} = 24.910814026057043$
$k_{\beta 4} = 33.100006712797217$
$k_{\beta 5} = -0.084498270977843237$
$k_{\beta 6} = 0.82350178698059129$
$k_{\beta 7} = 1460.6434072888394$
$k_{\beta 8} = -13642.429817870459$
$k_{\beta 9} = 20.499879869479599$
$k_{\beta 10} = -191.46916492500981$

Gains obtained for grid-connected operation:

$k_{\alpha 1} = -11.787063698397393$
$k_{\alpha 2} = 38.623131201840849$
$k_{\alpha 3} = 33.804866612214006$
$k_{\alpha 4} = 36.727007414250984$
$k_{\alpha 5} = -5891.889892297665$
$k_{\alpha 6} = 713.90691760765196$
$k_{\alpha 7} = 126.89103325043251$
$k_{\alpha 8} = -15.375098312742464$
$k_{\beta 1} = -38.623131202028887$
$k_{\beta 2} = -11.78706369828271$
$k_{\beta 3} = -36.72700741441944$
$k_{\beta 4} = 33.804866612323131$
$k_{\beta 5} = -713.9069180250807$
$k_{\beta 6} = -5891.8898947070456$
$k_{\beta 7} = 15.375098309609829$
$k_{\beta 8} = 126.89103325892579$

## Appendix B.

Table 1
Parameters of the laboratory rig

| Symbol | Parameter | Value |
|---|---|---|
| $P_n$ | Rated power | 7.5 kW |
| $U_s$ | Stator voltage | 220/380 V |
| $N_{sr}$ | Stator-to-rotor turns ratio | 380/182 |
| $R_s$ | Stator resistance | 0.43 Ω |
| $L_s$ | Stator leakage inductance | 12 mH |
| $R_r$ | Rotor resistance | 0.71 Ω |
| $L_r$ | Rotor leakage inductance | 12 mH |
| $L_m$ | Mutual inductance | 120 mH |
| $p$ | Pole pairs | 2 |
| $C_f$ | Stator filtering capacitance | 50 µF |